HAL
open science

Modelling the human pharyngeal airway: validation of numerical simulations using in vitro experiments

Franz Chouly, Annemie van Hirtum, Pierre-Yves Lagrée, Xavier Pelorson, Yohan Payan

To cite this version:

Franz Chouly, Annemie van Hirtum, Pierre-Yves Lagrée, Xavier Pelorson, Yohan Payan. Modelling the human pharyngeal airway: validation of numerical simulations using in vitro experiments. Medical and Biological Engineering and Computing, 2009, 47 (1), pp.49-58. 10.1007/s11517-008-0412-1 . hal-00340538

HAL Id: hal-00340538

https://hal.science/hal-00340538v1

Submitted on 26 Nov 2008

HAL is a multi-disciplinary open access archive for the deposit and dissemination of scientific research documents, whether they are published or not. The documents may come from teaching and research institutions in France or abroad, or from public or private research centers.

L'archive ouverte pluridisciplinaire **HAL**, est destinée au dépôt et à la diffusion de documents scientifiques de niveau recherche, publiés ou non, émanant des établissements d'enseignement et de recherche français ou étrangers, des laboratoires publics ou privés.

Medical & Biological Engineering & Computing manuscript No.
(will be inserted by the editor)

Franz Chouly · Annemie Van Hirtum · Pierre-Yves Lagrée · Xavier Pelorson · Yohan Payan

Modelling the human pharyngeal airway:

validation of numerical simulations using in-vitro experiments

Received: 09/05/08 / Accepted: 01/10/08

Abstract In the presented study, a numerical model which predicts the flow-induced collapse within the pharyngeal airway is validated using in-vitro measurements. Theoretical simplifications were considered to limit the computation time. Systematic comparisons between simulations and measurements were performed on an in-vitro replica, which reflects asymmetries of the geometry and of the tissue properties at the base of the tongue and in pathological conditions (strong initial obstruction). First, partial obstruction is observed and predicted. Moreover, the prediction accuracy of the numerical model is of 4.2 % concerning the deformation (mean quadratic error on the constriction area). It shows the ability of the assumptions and method to predict accurately and quickly a fluid-structure interaction.

Keywords numerical simulation and modelling · in-vitro measurements · fluid-structure interaction · obstructive sleep apnea syndrome

1 Introduction

Since the 90's, biomechanical modelling of the human upper airway has received a growing interest since it allows a better understanding of its physiology and pathophysiology, as well as an increased quality of the treatments of its specific pathologies. Among these, Obstructive Sleep Apnea Syndrome (OSAS) has been object of particular attention, as it became a major health care topic, affecting a growing part of the population, especifically in Europe and in the United States [22,39]. It is characterized by the occurence of an abnormal rate of apneas and hypopneas during sleep [22]. During an episode of obstructive apnea (respectively hypopnea), the soft tissue in the pharynx completely (respectively partially) collapses in response to

Franz Chouly
INRIA, REO team, Rocquencourt - BP 105, 78153 Le Chesnay Cedex, France.
Tel.: +33 (0)1 3963 5916
Fax.: +33 (0)1 3963 5882
E-mail: franz.chouly@inria.fr

Yohan Payan
Laboratoire TIMC, UMR CNRS 5525, Université Joseph Fourier,
38706 La Tronche, France.
E-mail: yohan.payan@imag.fr

Annemie Van Hirtum & Xavier Pelorson
Département Parole et Cognition, GIPSA-lab, INPG / UMR CNRS 5216,
46 Av. Felix Viallet, 38031 Grenoble, France.
E-mail: annemie.vanhirtum@gipsa-lab.inpg.fr / xavier.pelorson@gipsa-lab.inpg.fr

Pierre-Yves Lagrée
Institut Jean le Rond d'Alembert, UMR CNRS 7190,
4, Place Jussieu, 75252 Paris Cedex 05, France.
E-mail: pierre-yves.lagree@upmc.fr

inspiratory airflow. It induces a temporary cessation (respectively limitation) of the respiration [3]. The main health effects are excessive daytime sleepiness and an increased risk of cardiovascular diseases [22]. In parallel to the great amount of medical/biomedical engineering research that has been carried out to understand this highly complex phenomenon (see e.g. [38,1] for recent works or [22,3,12,9,10] for recent overviews), theoretical biomechanical models have been proposed such as simplified mathematical models of the interaction between the airflow and the soft tissue [13,11,2], numerical models of the respiratory fluid flow [28,19] and numerical models of the fluid-structure interaction [24,21,37]. They allow indeed to understand the relationship between the fluid-structure interaction in the pharynx and the abnormal flow patterns observed in the medical or physiological experiments. They might allow furthermore to predict these flow patterns using measurements of the biomechanical properties of the upper airway (geometry, rheology). This makes them of interest to improve the quality of the treatments such as surgical procedures [8,14] or mandibular advancement splints [15].

In a previous paper [6], a numerical model which aims at predicting the fluid-structure interaction within the pharyngeal airway has been described. It is based on simplified assumptions so that the computational cost of simulations be compatible with clinical applications. An original in-vitro tongue replica has also been described. It takes into account the very specific properties of the upper airway. In particular, the asymmetry of the pharyngeal duct at this level has been reproduced in a simplified manner. A few comparisons between predictions of the numerical model and measurements of the flow-induced collapse within the in-vitro replica provided encouraging results (see [6] for details). Nevertheless, this was not sufficent to be really conclusive about the interest and drawbacks of the numerical model. Therefore, the aim of this study was extensive validation of this numerical model through in-vitro experiments, and to our knowledge, it has not been done so far in this context (for instance in [37], the validation is carried out with rigid walls). The main novelty in comparison to the study presented in [6] is that systematic comparisons have been carried out, for a wide range of parameter values. Moreover, pressure sensors have been integrated into the experimental setup. As the pressure at the level of the constriction plays a critical role in the flow-induced collapse (see [34]), it was jugded interesting to assess its prediction in conditions of fluid-structure interaction. Besides, a digital camera quantifies the two-dimensional deformation of the simplified airway at the main site of obstruction. This gives more detailed and pertinent information than the laser beam which was of use in [6].

2 Material and methods

2.1 In-vitro setup

The aim of the experimental setup described here is to reproduce a fluid-structure interaction in conditions of strong obstruction and quasi-steady motion. It obviously simplifies the complex in-vivo reality, but allows to obtain reliable dynamical measurements of the pressure and of the deformation in controlled conditions, which is required for validation.

The in-vitro setup is depicted Figures 1 & 2. The real morphology of the upper airway has been simplified as suggested Figure 1 (a). However, its overall configuration and the main dimensions have been conserved. In particular, a frequent site of collapse is the base of the tongue [25]. This anatomical entity is represented in the setup by a short latex tube filled with water (deformable tongue replica). This deformable structure intersects orthogonally a rigid metallic pipe which stands for the pharynx. The geometry of the duct at the level of this junction is those of a constriction, in accordance with observations at the tongue base.

The diameter D of the deformable tongue replica is 49 mm. The latex wall (Piercan Ltd.) has a thickness e of 0.3 mm. Its Poisson's ratio ν is of 0.5 (incompressible material). The value of its Young modulus E has been determined to 1.68 MPa (see [4] for details). The latex sheet is mounted onto a rigid metallic support (Figure 2 (a)). A hole in the support enables the deformation of the latex in response to the fluid flow: the deformable part of the cylinder is depicted Figures 2 (a) & 1 (b) in dark shade. An external water supply (Figure 2 (c)) through a duct connected to a water column allows to control and to measure the water pressure P_{ext} inside the latex interface (external flow). Indeed, the height of the water column is controllable [33]. Manipulation of this pressure influences simultaneously two parameters: the geometry of the duct and the overall stiffness of the deformable part.

The rigid metallic pipe in which the airflow (internal flow) circulates is depicted Figure 2 (b). Its diameter d is of 25 mm. A removable flat plate allows to change the geometrical characteristics of the duct (Figure 1 (b)). Different heights[1] of the duct, corresponding to different pharyngeal calibers, can be chosen using different plates. Air supply comes from a pressure reservoir, which can be considered as an artificial lung. This is a rectangular box of approximatively 0.75 m^3, fed by a compressor. The control of the pressure in the reservoir is ensured by a pressure regulator (Norgren(TM) type 11-818-987). A constant selected pressure, within the range 0-3000 Pa, is thus obtained at the inlet of the duct [26]. The pressure within the airflow is measured with sensors located at different positions (Figure 1 (c)) One sensor (p_0) allows the measurement of the upstream pressure. Two others (p_1, p_2) are located at the bottom of the rigid plate, and allow measurements of the pressure at the level of the constriction and downstream. The pressure sensors are within holes of diameter 0.4 mm. They are piezo-electric[2] and deliver a tension proportional to the pressure. Preliminary calibration, with a liquid manometer (Kimo(TM)), allows to determine the constant of proportionality of the relationship. Then, the pressure is measured with a precision of $\pm$ 1 mmH_2O.

An important geometrical parameter is the minimal height of the duct, at the bottom of the upper cylinder, called the constriction height h_c (Figures 1 (b) (c) & 2 (c)). As explained before, this height could be changed using different metallic plates, while P_{ext} is maintained. In physiological terms, it corresponds to the minimal pharyngeal caliber. Another important parameter is the area at the level of the constriction A_c. It corresponds to the minimal pharyngeal area. We chose this parameter for the measurement of the flow-induced deformation since it captures its global effect on the obstruction of the duct (h_c is only a punctual measurement). To this purpose, a digital camera has been used (Figure 1 (c)), which measures the bidimensional geometry at the level of the constriction, in frontal view and at the downstream end (Figures 1 (b) & 2 (c)). The resulting information is the constriction height $h_c(z)$ for all z, from which we obtain the constriction area A_c and follow its variation.

The digital camera is an industrial model[3], with a resolution of 1280×1024 pixels. Its focal has been adjusted so as to visualize with the best accuracy the constriction site (focal plane located at the site of the constriction, and as wide as the rigid pipe). The zoom objective is such that the number of pixels corresponding to the constriction area is maximized. The contrast is enhanced with an ordinary light source upstream the pipe. A software[4] allows to control the parameters of the camera, to visualize and to store the resulting acquisitions. Those can be obtained automatically, at periodic time intervals, in synchronization with the pressure measurements, thanks to LabView[5]. A preliminary calibration is necessary, to determine the relationship between distances measured on the picture and real distances. The method consists in localizing three points on the picture. The distance between these points is known. After the calibration, the horizontal and vertical resolutions are determined: $r_h = r_v \simeq 6.3.10^{-3}$ cm / pixel.

2.2 Mechanical theory for fluid-structure interaction

Numerical computation of a complete fluid-structure interaction problem, i.e. solving the incompressible Navier-Stokes equations dynamically coupled with a deformable structure in large deformations, is still challenging nowadays, both in terms of stability and convergence towards the solution and in terms of computation cost [28, 18, 31, 35]. Therefore, the complexity of the description of the ongoing phenomena is reduced, and simplificatory assumptions are stated. The further outlined assumptions are made in agreement with the anatomy and the physiology of the upper airway, and they allow to reduce the computation time to a great extent. A detailled description of the biomechanical model and of the numerical method can be found in [6] and [4]. In this section, only the main characteristics are given.

---

[1] dimension in y direction
[2] *Endevco 8507C, Kulite XCS-093*
[3] *Inca 311, Philips*
[4] *Clicks(TM), version 1.4.0, Philips, Industrial Vision*
[5] LabView 7, National Instruments

Concerning the structure, the assumptions of a quasi-steady motion, with small deformations and displacements have been chosen. The constitutive behavior is given by the Hooke law (linear elasticity). As a result, the following equations govern the structure deformation:

$$\begin{cases} \nabla \cdot \boldsymbol{\sigma} + \mathsf{f} = 0, \\ \boldsymbol{\sigma} = \frac{E\nu}{(1-2\nu)(1+\nu)}\, \varepsilon_I \boldsymbol{I} + \frac{E}{1+\nu}\, \boldsymbol{\varepsilon}, \\ \boldsymbol{\varepsilon} = \frac{1}{2}(\nabla \mathsf{u} + (\nabla \mathsf{u})^t), \end{cases} \tag{1}$$

where $\boldsymbol{\sigma}$ is the Cauchy stress tensor, and f is the vector of external forces. E is the Young's modulus, and ν is the Poisson's ratio. ε_I is the trace (first invariant) of the small deformation tensor $\boldsymbol{\varepsilon}$. u is the vector of displacement. The boundary conditions consist in immobility constraints (displacement $\mathsf{u} = 0$) at sites of attachement to rigid parts and imposed external forces in the surface of contact with the airflow.

The fluid flow is considered as incompressible (Mach number of $O(10^{-2})$), laminar (Reynolds number of $O(10^3)$), stationnary (Strouhal number of $O(10^{-3})$) and bidimensional [34]. Since the Reynolds number is of the order of 10^3, we use an asymptotic simplification of the incompressible Navier-Stokes equations:

$$\begin{cases} \bar{u}\partial_{\bar{x}}\bar{u} + \bar{v}\partial_{\bar{y}}\bar{u} = -\partial_{\bar{x}}\bar{p} + \partial^2_{\bar{y}^2}\bar{u}, \\ -\partial_{\bar{y}}\bar{p} = 0, \\ \partial_{\bar{x}}\bar{u} + \partial_{\bar{y}}\bar{v} = 0, \end{cases} \tag{2}$$

$(\bar{u}, \bar{v})$ are the longitudinal $(\bar{x})$ and transverse $(\bar{y})$ components of the fluid velocity, and $\bar{p}$ is the pressure [17]. All the variables are nondimensional: $\bar{x} = x(h_0 Re)^{-1}$, $\bar{y} = y h_0^{-1}$, $\bar{p} = P(\rho U_0^2)^{-1}$, $\bar{u} = u U_0^{-1}$, $\bar{v} = v Re U_0^{-1}$; where h_0 is the transversal dimension of the pharyngeal duct, U_0 is the mean longitudinal speed, and Re is the Reynolds number ($Re = U_0 h_0/\nu$, with ν the kinematic viscosity of the air). These equations, called Reduced Navier-Stokes / Prandtl (RNSP), allow to take into account the boundary layer formation as well as the separation of the fluid after the narrowing of the pharyngeal duct, at the base of the tongue [17]. The boundary conditions are the following: no slip on the upper and lower walls and a pressure difference ΔP imposed between the inlet and the outlet.

2.3 Numerical solving of the equations

As the problem is considered as quasi-steady, the fluid-structure interaction is solved using a segregative method: the equations that govern the fluid and the solid are solved alternatively, inside a global loop. The pressure gradient in the fluid is imposed gradually, in st steps : $\Delta P_1 = 0, \ldots, \Delta P_{st} = \Delta P_{max}$. For each pressure gradient ΔP_i at step i, the fluid forces on the wall are first computed and imposed. Then, the wall is deformed, which changes the fluid flow domain. The fluid forces need then to be computed again. This is the reason why a finite number of iterations it should be imposed at each step, until equilibrium of the wall is reached. A convergence criterion cv, which corresponds to the maximal displacement between two iterations, allows to ensure that at the end of the it iteration, the displacement of the structure is no more significant. Typically, a choice of $st = 8$ and $it = 6$ has been found sufficient to ensure the convergence of the algorithm ($cv \simeq 10^{-3}$ mm).

The continuum equations of the wall are solved using the finite element method [40]. In the context of small deformations and of linear elasticity, the relationship between the nodal displacements and the nodal forces is linear. As a result, the precomputation of the inverse of the stiffness matrix $[\mathbf{K}]$ is done before the fluid-structure interaction loop [7]. It saves computation time as nodal displacements are obtained through simple matrix multiplication at each iteration. This preliminary step is achieved using a commercial finite element solver (Ansys(TM) Software). The finite element model of the tongue replica, in other terms of the latex tube filled with water, is depicted Figure 3. The mesh is constituted of 150 linear elements of 8 nodes, regularly dispatched. The nodes in contact with the hollow metal support (Figure 2 (a)) are immobilized (Figure 3). The boundary conditions are such that a bidimensional model would have not been satisfying. This is the reason for the choice of a tridimensional model. The incompressibility of the latex is approximated through the choice

of a Poisson's ratio ν of 0.499. The Young modulus has been fixed to $E = 1.68$ MPa. The water inside the latex tube has been taken into account in the model through the application of constant pressure forces on the surfaces supposed to be in contact with the water.

The RNSP equations that govern the fluid flow are solved using a finite difference method [16], which is easy to implement and allows fast numerical solving. The grid that is used is of size 2000×1000. This is sufficently high to capture boundary layer formation and separation, as well as jet formation, and increasing the grid resolution above this level does not significantly change the values of the pressure distribution (see [4] and [6] for details). As the airflow is modelled using bidimensional equations, the finite element model is divided into 5 thin slices on which are carried out computations of the fluid forces. A finite element model of 10 slices has also been built so as to check the impact of this numerical parameter and no significant difference between the two models has been found. The resulting pressure distribution is imposed at the surface of the structure in agreement with the principle of virtual works, which provides an accurate approximation of the pressure load (see [6] for detailed formulas). The codes for computation of the fluid flow and fluid-structure interaction have been written by the authors, using Matlab(TM) interfaced with C language. As a result, the duration of the computations for the overall algorithm is typically of the order of 20 minutes[6]. This can be considered as reasonable for clinical applications.

2.4 Methodology for comparisons

A batch of measurements has been carried out, for which the latex thickness ($e = 0.3$ mm) and the initial constriction height ($h_c^0 = 1.84$ mm)[7] remained fix. The following parameters were systematically varied:

- the external pressure P_{ext},
- the maximal inlet pressure P_e^{max}.

The external pressure ranges from 100 to 700 Pa. For each value of P_{ext}, four measurements have been carried out, corresponding to different values of P_e^{max} : 200, 400, 600 and 800 Pa. Measurements are performed according to the following procedure: the inlet pressure P_e is gradually increased from 0 Pa up to the required value P_e^{max}. At fixed time steps (0.25 s), a synchronized sampling of the following outputs is done automatically:

- the upstream pressure P_e, the pressure P_c^0 at $x = 0$ mm, and the pressure P_c^{16} at $x = 16$ mm, as measured respectively by the sensors p_0, p_1, p_2 described in Section 2.1. Note that when $P_e = 0$ Pa, P_c^0 corresponds to the pressure at the level of the constriction. Yet, during the deformation, the new position of the wall can be such that the pressure P_c^0 does no longer correspond to the pressure at the constriction.
- the height of the duct at the level of the constriction : $h_c(z)$, using the digital camera described in Section 2.1. The constriction area A_c is determined automatically.

The experiment is stopped when the value observed for the output does not change anymore. The stationnary state is then reached, after approximatively 10 seconds.

For each value of P_{ext}, the mean experimental curves $P_c^{0,exp}(P_e)$ and $A_c^{exp}(P_e)$ that result from the four experiments at different values of P_e^{max} are computed, with the associated standard deviation. A numerical simulation is then carried out. The inlet pressure in the simulation is equal to P_e and the outlet pressure is equal to P_c^{16}. The theoretical curves $P_c^{0,sim}(P_e)$ and $A_c^{sim}(P_e)$ are compared to the experimental ones: $P_c^{0,exp}(P_e)$ and $A_c^{exp}(P_e)$. For quantitative comparison we compute first the mean quadratic error, in normalized form, which is, for the constriction area:

$$\tilde{\varepsilon}_2(A) = \frac{1}{A_c^{P^{ext}}} \left[\frac{1}{n} \sum_{i=1}^{n} \left(A_c^{exp}(P_e^i) - A_c^{sim}(P_e^i) \right)^2 \right]^{\frac{1}{2}} . \tag{3}$$

Here, n is the number of points in the experimental sample, $(P_e^i, A_c^{exp}(P_e^i))$ the coordinates of the ith experimental point, $(P_e^i, A_c^{sim}(P_e^i))$ the coordinates of the corresponding point on the theoretical curve. The constant of normalization $A_c^{P^{ext}}$ is the area at the beginning of the experiment, when no internal airflow is circulating

[6] Dell Precision 330 (TM) workstation, with Pentium(TM) 4, 2 GHz, 1 GO RAM.
[7] at $P_{ext} = 0$ Pa

($P_e = 0$ Pa) and after a water pressure P_{ext} has been imposed. For the pressure P_c^0, the quadratic error $\tilde{\varepsilon}(P^0)$ is computed identically, except the constant of normalization which is the maximal inlet pressure: P_e^{max}. A maximal error has been computed as well:

$$\tilde{\varepsilon}_{max}(A) = \frac{1}{A_c^{P_{ext}}} \max_{1 \leq i \leq n} \left| A_c^{exp}(P_e^i) - A_c^{sim}(P_e^i) \right|, \tag{4}$$

(and an identical definition for $\tilde{\varepsilon}_{max}(P^0)$). Finally, the overall prediction performance is evaluated using the coefficient of determination R^2 ($0 \leq R^2 \leq 1$):

$$R^2 = 1 - \frac{\hat{\sigma}^2}{\sigma_y^2}, \tag{5}$$

$\hat{\sigma}^2$ being the variance of the prediction residuals, and σ_y^2 is the variance of the experimental measurements. The closer is R^2 to 1, the best is the prediction of the numerical simulation. As a result, two coefficients of determination are computed: R_P^2 for the pressure at the level of the (initial) constriction $x = 0$ and R_A^2 for the constriction area.

3 Results

The results of the comparisons between predictions and measurements are summarized Table 1, for all the investigated values of P_{ext}, and a typical example of the resulting curves $P_c^0(P_e)$ and $A_c(P_e)$ is given Figure 4, for $P_{ext} = 300$ Pa. First, it should be noticed that the measurements are strongly repeatable. Table 1 indicates a mean value of the standard deviation σ_{exp}, computed from the four repeated measurements, of 11.3 Pa for the pressure P_c^0 and of 0.29 mm^2 for the constriction area A_c. Variations of this standard deviation with P_e can be observed Figure 4.

First, concerning the pressure P_c^0 at $x = 0$ mm, the theoretical and experimental curves are in agreement with a mean error of less than 8 %, until P_e exceeds 500 Pa. After this value, they split, and the value of the computed pressure is always lower than the experimental value (of $\simeq 30$ %, see Figure 4 (a)). Moreover, this pressure is both negative and decreasing at the origin, but quickly changes to become positive and increasing. This could be explained by the translation of the constriction towards downstream as P_e is increased and the wall is deformed. As a result, the pressure P_c^0 moves away from the value of the pressure at the constriction, that remains still negative. The most valuable explaination for the difference observed between the theoretical and the experimental values of P_c^0 is that the simulation underestimates the displacement of the wall in the x direction. Considering the shape of the curve $P(x)$ in the area of the constriction, an error of the order of 1 mm in the prediction of the displacement should be followed by an error of the order of 100 Pa in the prediction of the pressure. These phenomena lead to a mean quadratic error of 9.8 % and a mean value for R_P^2 of 0.64 (see Table 1).

Then, concerning the constriction area A_c, the mean quadratic error is of 4.2 % ($R_A^2 = 0.71$). The theoretical and experimental curves are depicted Figure 4 (b). At the origin ($P_e = 0$ Pa), there is no significant error between theory and experiments. This is not surprising since the values of A_c for $P_e = 0$ Pa and all the values of P_{ext} have been used to determine a Young modulus that gives the best adequation between simulations and data (see [4]). For values of P_e between 0 Pa and 200 Pa ($0 \leq Re \leq 1000$), a plateau is observed in the experimental curves. It is explained by inertial effects in the deformable portion, which are not taken into account in the model because of the assumption of quasi-static deformation. Nevertheless, it is not the major source of difference between the theoretical and experimental curves. For $200 \leq P_e \leq 400$ Pa ($1000 \leq Re \leq 1400$), A_c is a decreasing function of P_e. This function, in a first approximation, should be treated as linear. In this range of values of P_e, the agreement between theory and experiments can be considered as satisfying. The maximal amplitude of the closure ($\Delta A_c^{max}/A_c(P_e = 0)$) is of approximatively 18 %, and does not change significantly with P_{ext}. This maximal closure is always obtained for $P_e \simeq 400$ Pa. Indeed, in the interval ($400 \leq P_e \leq 700$ Pa, $1400 \leq Re \leq 1900$), a change is observed: the duct reopens at the level of the constriction. This behaviour might be explained by an increase of the downstream pressure $P_c^{16,exp}$ (up to $\simeq 180$ Pa, after $P_e = 400$ Pa). As $P_c^{16,exp}$ is used in the simulations to impose the values of the outlet pressure P_s, the numerical model is able to reproduce this reopening, though the strong non-linearity in the experimental curves is not reproduced

in the simulations. In the last interval ($P_e \geq 700$ Pa, $Re \geq 1900$), the theoretical and experimental curves are diverging. Indeed, after this critical value of Re, self-sustained oscillations in the latex structure are initiated. No measurement of A_c is possible in this case. As the modelling assumptions include quasi-steadiness, such a behaviour can not be reproducted by the simulations.

4 Discussion

First, in the in-vitro experiments, flow-induced obstruction has been observed systematically, with a ratio $\Delta A_c^{max}/A_c(P_e = 0)$ of approximatively 18 %. This confirms the preliminary experimental results of [6]. This effect is due to the internal airflow, which is submitted to acceleration at the level of the constriction and induces pressure losses (Venturi effect). Since the deformation of the latex wall is governed by the local pressure difference between the internal and external flow, these pressure losses result in a decrease of the constriction area (partial obstruction of the duct). The values of the couple (P_e, P_s) during an experiment are such that in the quasi-steady regime ($200 \leq P_e \leq 400$ Pa), the expiratory phase is reproduced in a very simplified manner. Remembering the analogy between the latex cylinder and the base of the tongue, the airflow which circulates in the pipe is similar to an airflow which would go from the hypopharynx to the mouth cavity. P_e would then be the pressure in the hypopharynx, at the base of the epiglottis, and P_s the pressure in the mouth cavity, approximatively equal to the atmospheric pressure (as in the simplified models described in [20,36]). Considering this analogy as valid, the presented experiments would then reproduce the flow-induced obstruction in conditions of expiratory flow, which has been observed in some apneic patients or heavy snorers, and may be at the origin of expiratory flow limitation [23,27,30,36]. This analogy, already dicussed in [6], is however limited, since the experiments do not reproduce with accuracy the complex dynamics of a respiratory cycle (see e.g. [38]), and was only focused on the quasi-steady phenomena. The range of values of the upstream pressure P_e, however, is physiological as it conduces to airflow rates of the order of 10 l/min (see e.g. [32]). As a result, an extensive study of the response of the tongue replica to different pressure commands, close to some typical physiological or pathophysiological cases, may constitute a first perspective of this work. In particular, measurements in conditions closer to inspiration (P_e equals to the atmospheric pressure, and $P_s < P_e$) would allow to reproduce in a simplified manner what happens during an apneic episode, which is known to occur during the inspiratory phase. Of course, the change from expiration to inspiration corresponds to a simple change of boundary conditions in the numerical model, and simulations in inspiratory configuration have been carried out with success from medical data (sagittal radiographies) [5]. Nevertheless, experiments in inspiratory configuration would be of interest, on the one hand, to validate the simulations in this case, and on the other, to obtain deformations of the latex structure of larger amplitudes. Furthermore, considering the actual geometry of the setup, it is impossible to obtain a complete closure of the channel, which would be of interest as Obstructive Sleep Apnea is associated to complete closure of the pharynx and complete flow cessation.

Then, concerning the main point of this study, which is the experimental validation of the numerical model described in Section 2, this one can be considered to provide a satisfying first approximation for the prediction of the flow-induced collapse measured with the in-vitro setup. Indeed, the main quadratic error for the prediction of the constriction area is of 4.2 % ($R_A^2 = 0.71$). This error does not vary significantly with the pressure P_{ext} in the external flow, when $P_{ext} \leq 500$ Pa. For $P_{ext} = 700$ Pa, this error is higher and thus this value can be considered as a limit of validity for the numerical model. Moreover, the theoretical and experimental curves are in good adequation for the range of values of P_e (200-400 Pa) corresponding to quasi-steady behaviour and thus relevant to our study. When the upstream pressure is higher ($P_e \simeq 700$ Pa), auto-oscillations are observed in the experiments. This behaviour has already been reported on symmetrical [26] as well as on asymmetrical geometries [6]. It can be predicted using linear stability theory in association with a simplified physical model [26]. In our case and according to the assumption of quasi-steadiness, this phenomenon can not be reproduced in the simulations. However, it should be associated to snoring or speech production processes, and is therefore not relevant here. The simplified asymptotic theory (RNSP) to model the fluid may be the first cause of the differences between numerical predictions and measurements. However, systematic comparisons effectuated with help of a rigid tongue replica proved that this theory provides an accurate prediction of the pressure distribution for the geometry we used, even if the assumption of small variations in the axial direction necessary to derive the equations is not satisfied [34]. From the earlier study [34], it resulted also that the recirculation effects as well as turbulent effects that may occur after separation of the flow had negligible impact on the prediction of the pressure distribution. Moreover, no evidence of turbulence has been found

in the region upstream the point of flow separation [34]. The assumptions stated for the structure explain the other part of the discrepancies between theory and experiments. In particular, the measurement of the pressure at the level of the (initial) constriction ($x = 0$ mm) revealed that the numerical model underestimates the displacement of the tongue replica. This might be due to the assumption of small displacements which is not respected in this situation. An improvement would then consist in using a shell or membrane theory with the assumption of large displacements (geometrical non-linearity) for the finite element simulation. Yet, this phenomenon does not have a strong effect on the final prediction of the flow-induced obstruction.

The in-vitro setup allows to measure the pressure and the deformation during a fluid-structure interaction, in a configuration with strong asymmetry. Because of this asymmetry, the setup remains much more appropriate than other previous physical models, such as the collapsible tube (see e.g. [3, 29]), to study the human pharyngeal airway. Furthermore, the measurement of the pressure at the level of the constriction, which plays a critical role in the flow-induced collapse, coupled to the measurement of the bidimensional geometry of the duct at the constriction, permitted to refine the results and analysis carried out in [6]. Nevertheless, as a simplification of the complex physiological reality, this setup has some limitations. For instance, it neglects the tridimensional effects that should be involved in a true human airway, where lateral walls seem to play a role during the collapse [3]. In the protocol, it would also be interesting to measure the lateral deformation of the tongue replica, so as to compare it to the numerical prediction. More pressure sensors would also help to capture with more accuracy the pressure distribution.

Finally, concerning the clinical implications of this work, the numerical model proposed, as other models based on continuum mechanics (see e.g. [22]), is able to take into account easily and with relative accuracy patient-specific geometrical and mechanical properties. In particular, the choice of the Hooke law to model the soft tissue is reasonable for patient-specific modelling, since it appears difficult to obtain more information than the Young modulus from in-vivo measurements. A second advantage of the proposed model is that the simulation time is reduced due to the simplificatory assumptions. It is of the order of 20 min on a standard computer[8], which may already be satisfying for a physiologist or a clinician. With a simple optimization of the code, still in a preliminary version, this time would be expected to be the order of one minute. At last, the in-vitro validation described in this paper should normally be an argument so that a clinician or a physiologist may trust the predictions from the numerical model, though in-vivo validation in this perspective is a must and remains our ultimate goal.

5 Conclusion

Extensive experimental validation of a numerical model that predicts the flow-induced collapse of the pharyngeal airway in conditions of strong obstruction has been carried out. An in-vitro setup which reproduces the asymmetries and the particularities of the airway at the base of the tongue in pathological conditions has been used for this purpose. The prediction accuracy for the obstruction is of 4.2 % (mean quadratic error between prediction and measurements concerning the variation of the constriction area), and has been assessed for a wide range of parameter values. Then, it results from these comparisons that the numerical model may be considered as satisfying in a first approximation to predict the flow-induced deformation. Since it is based on simplified assumptions, a low computational cost is associated to each numerical simulation, which is an advantage for clinical applications.

Acknowledgements The authors would like to thank Pierre Chardon, Yves Garnier and Freek van Uittert (Technische Universiteit Eindhoven, Netherlands) for their very precious help on the in-vitro setup. They would like also to thank Pr. Jean-Roch Paoli, Pr. Bernard Lacassagne and Pr. Michel Tiberge (CHU Purpan, Toulouse, France) for their help on medical aspects.

References

1. Abeyratne, U., Karunajeewa, A., Hukins, C.: Mixed-phase modeling in snore sound analysis. Med Biol Eng Comp **45**, 791–806 (2007)

[8] Dell Precision 330 (TM) workstation, with Pentium(TM) 4, 2 GHz, 1 GO RAM.

2. Aittokallio, M., Gyllenberg, M., Polo, O.: A model of a snorer's upper airway. Math Biosci **170**, 79–90 (2001)
3. Ayappa, I., Rapoport, D.M.: The upper airway in sleep : physiology of the pharynx. Sleep Med Rev **7**(1), 9–33 (2003)
4. Chouly, F.: Modélisation physique des voies aériennes supérieures pour le Syndrome d'Apnées Obstructives du Sommeil. Ph.D. thesis, I.N.P.G. - Grenoble (2005)
5. Chouly, F., Van Hirtum, A., Lagrée, P.Y., Paoli, J.R., Pelorson, X., Payan, Y.: Simulation of the retroglossal fluid-structure interaction during obstructive sleep apnea. LNCS **4072**, 48–57 (2006)
6. Chouly, F., Van Hirtum, A., Lagrée, P.Y., Pelorson, X., Payan, Y.: Numerical and experimental study of expiratory flow in the case of major upper airway obstructions with fluid-structure interaction. J Fluid Struct **24**, 250–269 (2008)
7. Cotin, S., Delingette, H., Ayache, N.: Real-time elastic deformations of soft tissues for surgery simulation. IEEE Trans Visu Comp Graph **5**(1), 62–73 (1999)
8. Crampette, L., Carlander, B., Mondain, M., Billiard, M., Guerrier, B., Dejean, Y.: Surgical alternatives to uvulopalatopharyngoplasty in sleep apnea syndrome. Sleep **15**(6), S63–S68 (1992)
9. Fairbanks, D., Mickelson, S., Woodson, B. (eds.): Snoring and Obstructive Sleep Apnea (3rd Edition). Lippincott Williams and Wilkins (2003)
10. Ferber, R. (ed.): Progress in Sleep Apnea Research. Nova Science Publishers (2007)
11. Fodil, R., Ribreau, C., Louis, B., Lofaso, F., Isabey, D.: Interaction between steady flow and individualised compliant segments: application to upper airways. Med Biol Eng Comp **35**, 1–11 (1997)
12. Fogel, R.B., Malhotra, A., White, D.P.: Sleep - 2: Pathophysiology of obstructive sleep apnoea/hypopnoea syndrome. Thorax **59**, 159–163 (2004)
13. Gavriely, N., Jensen, O.E.: Theory and measurements of snores. J Appl Phys **74**(6), 2828–2837 (1993)
14. Guilleminault, C., Quera-Salva, M.A., Powell, N.B., Riley, R.W.: Maxillo-mandibular surgery for obstructive sleep apnoea. Eur Resp J **2**, 604–612 (1989)
15. Hui, D.S.C., Choy, D.K.L., Ko, F.W.S., Li, T.S.T., Lai, C.K.W.: Obstructive sleep apnoea syndrome : treatment update. HKMJ **6**(2), 209–217 (2000)
16. Lagrée, P.Y., Berger, E., Deverge, M., Vilain, C., Hirschberg, A.: Characterization of the pressure drop in a 2D symmetrical pipe: some asymptotical, numerical and experimental comparisons. ZAMM **85**(2), 141–146 (2005)
17. Lagrée, P.Y., Lorthois, S.: The RNS/Prandtl equations and their link with other asymptotic descriptions: application to the wall shear stress scaling in a constricted pipe. Int J Eng Sci **43**, 352–378 (2005)
18. Li, Z., Kleinstreuer, C.: Blood flow and structure interactions in a stented abdominal aortic aneurysm model. Med Eng Phys **27**, 369–382 (2005)
19. Liu, Z., Luo, X., Lee, H., Lu, C.: Snoring source identification and snoring noise prediction. J Biomech **40**(4), 861–870 (2007)
20. Lofaso, F., Lorino, A., Fodil, R., Pia D'Ortho, M., Isabey, D., Lorino, H., Goldenberg, F., Harf, A.: Heavy snoring with upper airway resistance syndrome may induce intrinsic positive end-expiratory pressure. J Appl Phys **85**, 860–866 (1998)
21. Malhotra, A., Huang, Y., Fogel, R.B., Pillar, G., Edwards, J.K., Kikinis, R., Loring, S.H., White, D.P.: The male predisposition to pharyngeal collapse. AJRCCM **166**, 1388–1395 (2002)
22. Malhotra, A., White, D.P.: Obstructive Sleep Apnoea. The Lancet **360**, 237–245 (2002)
23. Martin, R.J., Pennock, B.E., Orr, W.C., Sanders, M.H., Rogers, R.M.: Respiratory mechanics and timing during sleep in occlusive sleep apnea. J Appl Phys **48**(3), 432–437 (1980)
24. Payan, Y., Chabanas, M., Pelorson, X., Vilain, C., Levy, P., Luboz, V., Perrier, P.: Biomechanical models to simulate consequences of maxillofacial surgery. CRAS **325**, 407–417 (2002)
25. Rama, A.N., Tekwani, S.H., Kushida, C.A.: Sites of obstruction in obstructive sleep apnea. Chest **122**(4), 1139–1147 (2002)
26. Ruty, N., Pelorson, X., Van Hirtum, A., Lopez-Arteaga, I., Hirschberg, A.: An in vitro setup to test the relevance and the accuracy of low-order vocal folds models. JASA **121**, 479–490 (2007)
27. Sanders, D., Moore, S.: Inspiratory and expiratory partitioning of airway resistance during sleep in patients with sleep apnea. Am Rev Resp Dis **127**, 554–558 (1983)
28. Shome, B., Wang, L.P., Santare, M.H., Prasad, A.K., Szeri, A.Z., Roberts, D.: Modeling of airflow in the pharynx with application to sleep apnea. J Biom Eng **120**, 416–422 (1998)
29. Smith, P.L., Wise, R.A., Gold, A.R., Schwartz, A.R., Permutt, S.: Upper airway pressure-flow relationships in obstructive sleep apnea. J Appl Phys **64**(2), 789–795 (1988)
30. Stănescu, D., Kostianev, S., Sanna, A., Liistro, G., Veriter, C.: Expiratory flow limitation during sleep in heavy snorers. Eur Resp J **9**, 2116–2121 (1996)
31. Tada, S., Tarbell, J.M.: A computational study of flow in a compliant carotid bifurcation-stress phase angle correlation with shear stress. Ann Biom Eng **33**(9), 1202–1212 (2005)
32. Trinder, J., Kay, A., Kleiman, J., Dunai, J.: Gender differences in airway resistance during sleep. J. Appl. Physiol. **83**(6), 1986–1997 (1997)
33. Van Hirtum, A., Cisonni, J., Ruty, N., Pelorson, X., Lopez, I., van Uittert, F.: Experimental validation of some issues in lip and vocal fold physical models. Acta Acustica **93**(2), 314–323 (2007)
34. Van Hirtum, A., Pelorson, X., Lagrée, P.Y.: In vitro validation of some flow assumptions for the prediction of the pressure distribution during obstructive sleep apnoea. Med Biol Eng Comp **43**, 162–171 (2005)
35. Wolters, B.J.B.M., Rutten, M.C.M., Schurink, G.W.H., Kose, U., de Hart, J., van de Vosse, F.N.: A patient-specific computational model of fluid-structure interaction in abdominal aortic aneurysms. Med Eng Phys **27**(10), 871–883 (2005)
36. Woodson, B.: Expiratory pharyngeal airway obstruction during sleep: a multiple element model. Laryngoscope **113**, 1450–1459 (2003)
37. Xu, C.: Computational mechanics models for studying the pathogenesis of obstructive sleep apnea (OSA). Ph.D. thesis, Drexel University, United States (2005)

38. Yamashiro, S.: Non-linear dynamics of human periodic breathing and implications for sleep apnea therapy. Med Biol Eng Comp **45**, 345–356 (2007)
39. Young, T., Palta, M., Dempsey, J., Skatrud, J., Weber, S., Badr, S.: The occurence of sleep-disordered breathing among middle-aged adults. New Engl J Med **328**(17), 1230–1235 (1993)
40. Zienkiewicz, O.C., Taylor, R.L.: The finite element method. Basic formulation and linear problems. McGraw-Hill Book Company (1989)

$P_{ext}(Pa)$	100	200	300	500	700	Mean	
$P^0_{c,exp}(P_e^{max})$ (Pa)	543	549	544	619	545	560	
$P^0_{c,num}(P_e^{max})$ (Pa)	301	347	369	427	444	377	
$\sigma_{exp}(P)$ (Pa)	11.3	11.0	10.9	12.1	11.2	11.3	(a)
$\tilde{\varepsilon}_2(P)$ (%)	11.2	9.8	9.2	9.2	9.9	9.8	
$\tilde{\varepsilon}_{max}(P)$ (%)	16.5	15.2	14.3	13.7	15.0	14.9	
R^2_P	0.43	0.53	0.58	0.76	0.88	0.64	

$P_{ext}(Pa)$	100	200	300	500	700	Mean	
ΔA_c^{max} (mm^2)	5.96	5.42	5.16	4.64	3.60	4.95	
$\sigma_{exp}(A)$ (mm^2)	0.26	0.30	0.29	0.27	0.31	0.29	
$\tilde{\varepsilon}_2(A)$ (%)	3.2	3.1	3.2	4.1	7.2	4.2	(b)
$\tilde{\varepsilon}_{max}(A)$ (%)	6.0	6.1	6.5	7.4	12.6	7.7	
R^2_A	0.78	0.83	0.72	0.67	0.53	0.71	

Table 1 Comparison between the predictions and the measurements of the pressure at the constriction P_c^0 (a) and the constriction area A_c (b), for different values of P_{ext}.

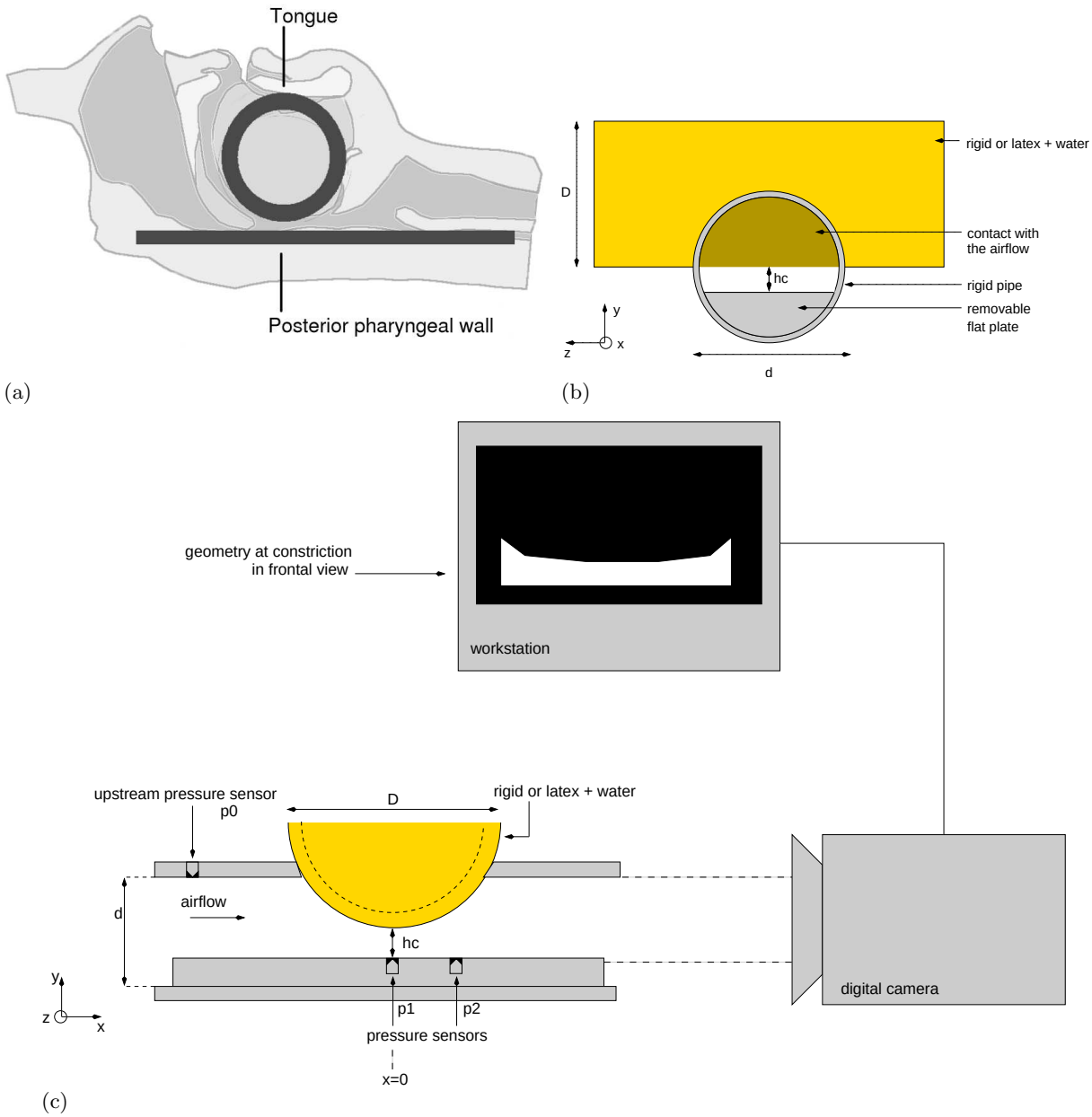

Fig. 1 Sagittal view of the upper airway overlaid with an outline of the in-vitro setup (a). Outline of the in-vitro setup, from frontal view (b). Experimental measurement of the wall deformation with a digital camera (c). The acquisitions of the camera are treated automatically with a software. Pressure sensors allow to obtain at each time step information about the airflow, which complements the information that comes from the camera.

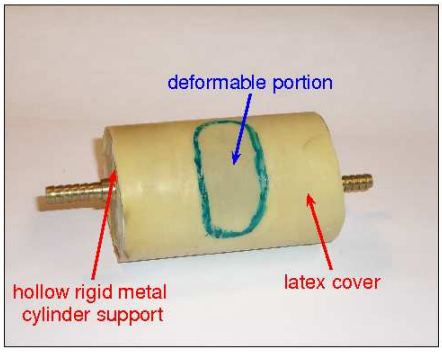

(a)

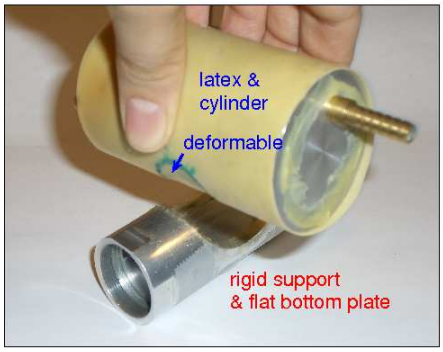

(b)

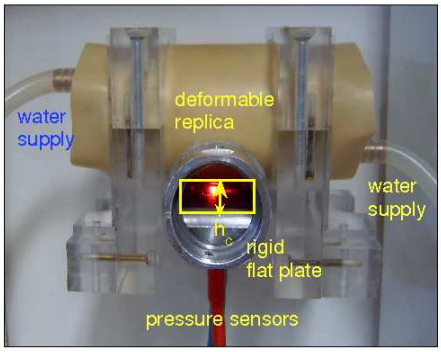

(c)

Fig. 2 Photographs of the in-vitro setup. (a) Deformable upper cylinder: view of the deformable portion. (b) The mounting of the 'in-vitro' tongue replica. (c) Frontal view of the replica at downstream end.

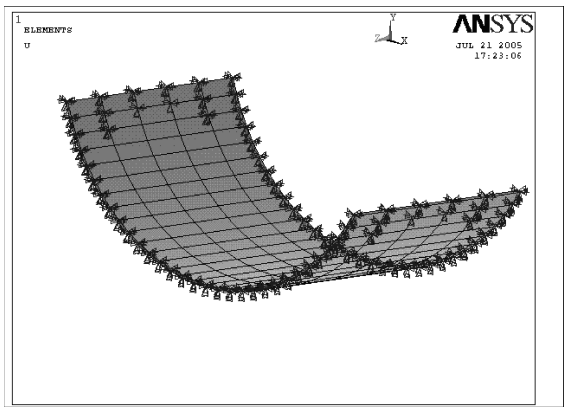

Fig. 3 Finite element model of the latex wall of the in-vitro setup, with boundary conditions. The nodes indicated by black arrows are immobilized, as they are supposed to be fixed to the rigid pipe.

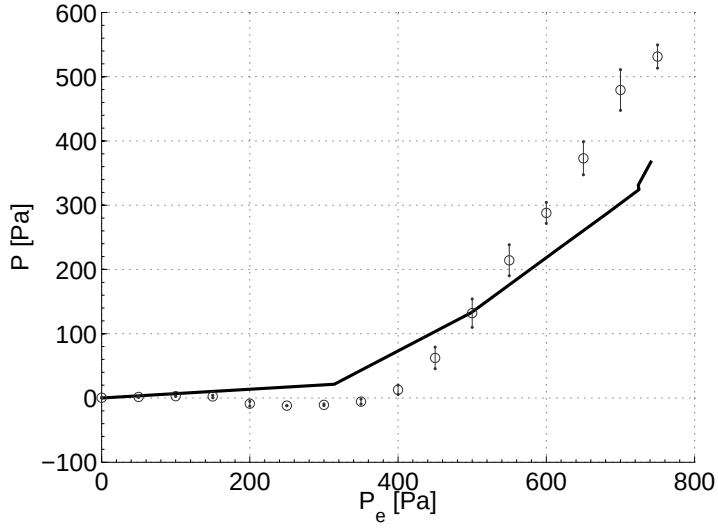

(a)

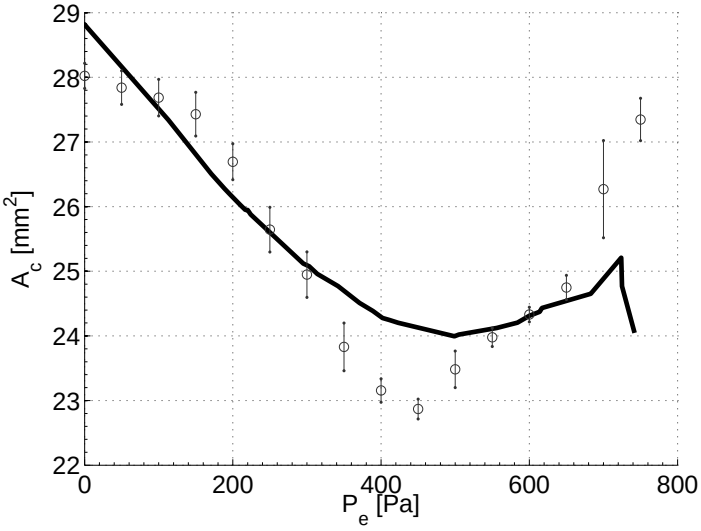

(b)

Fig. 4 Example of a comparison between the measurements (mean value with standard deviation, in grey) and the simulations (black curve) for $P_{ext} = 300$ Pa. The pressure P_c^0 (a) and the constriction area A_c (b) are compared.